Optics & Laser Technology 79 (2016) 24–31

Contents lists available at ScienceDirect

Optics & Laser Technology

journal homepage: www.elsevier.com/locate/optlastec

Full length article

Nonlinear optical studies of inorganic nanoparticles–polymer nanocomposite coatings fabricated by electron beam curing

Nilanjal Misra [a,*], Mounika Rapolu [b], S. Venugopal Rao [b,*], Lalit Varshney [a,c], Virendra Kumar [a,c]

[a] Radiation Technology Development Division, Bhabha Atomic Research Centre, Mumbai 400085, India
[b] Advanced Centre of Research in High Energy Materials (ACRHEM), University of Hyderabad, Hyderabad 500046, Telangana, India
[c] Homi Bhabha National Institute, Anushaktinagar, Mumbai 400094, India

ARTICLE INFO

Article history:
Received 8 September 2015
Received in revised form
14 October 2015
Accepted 5 November 2015

Keywords:
Optical limiting
Silver nanoparticles
Polymer nanocomposites
Electron beam
Picosecond
Femtosecond
Z-scan

ABSTRACT

The optical nonlinearity of metal nanoparticles in dielectrics is of special interest because of their high polarizability and ultrafast response that can be utilized in potential device applications. In this study nanocomposite thin films containing in situ generated Ag nanoparticles dispersed in an aliphatic urethane acrylate (AUA) matrix were synthesized using electron beam curing technique, in presence of an optimized concentration of diluent Trimethylolpropanetriacrylate (TMPTA). The metal nanocomposite films were characterized using UV–visible spectrophotometry, transmission electron microscope (TEM) and field emission scanning electron microscope (FE-SEM) techniques. Ag nanoparticle impregnated films demonstrated an absorption peak at ~420 nm whose intensity increased with increase in the Ag concentration. The optical limiting property of the coatings was tested using a nanosecond Nd-YAG laser operated at third harmonic wavelength of 355 nm. For a 25 ns pulse and 10 Hz cycle, Ag-polymer coatings showed good optical limiting property and the threshold fluence for optical limiting was found to be ~3.8×10^{-2} J/cm^2 while the transmission decreased to 82%. The nonlinear optical coefficients were also determined using the standard Z-scan technique with picosecond (~2 ps, 1 kHz) and femtosecond (~150 fs, 100 MHz) pulses. Open aperture Z-scan data clearly suggested two-photon absorption as the dominant nonlinear absorption mechanism. Our detailed studies suggest these composites are potential candidates for optical limiting applications.

1. Introduction

The use of high power lasers operating over a wide range of wavelengths and pulse durations has become widespread in recent years. This increase in the applications of lasers has led to a simultaneous growth in the need for optical limiters, which are indispensable in the context of protection of optical components and the human eye from laser-induced damages. An ideal optical limiter is defined as a device which exhibits appreciable linear transmission below a threshold input fluence and a constant transmission above it [1]. Therefore, over the years numerous materials have been discovered and developed for use as optical limiters. These include materials such as phthalocyanines, porphyrins, fullerenes, carbon nanotubes, organic dyes, metal nanoclusters, etc. [2–7]. Metal nanoparticles and nanocomposites have, in recent years, received significant attention owing to their unique nonlinear optical (NLO) properties, such as two-photon absorption (TPA), saturable absorption (SA), reverse saturable absorption (RSA), and self-focusing/defocusing arising from nonlinear refraction [8–14]. These NLO properties find application in the design and development of many photonics based devices for optical switching and optical signal processing of information at an enhanced speed compared to electronic counterparts. Materials with ultrafast time response (ideally in the sub-picosecond regime), strong nonlinearity (high value of nonlinear refractive index for optical switching applications and high value of nonlinear absorption for optical limiting and Q-switching kind of applications) combined with high resistance to bulk and surface laser damage are the key requirements for implementation of such high end applications. Therefore, detailed studies of novel materials are essential wherein the effects of pulse duration, wavelength, etc. should be thoroughly investigated. In this regard metal nanoparticles dispersed in polymer matrices have resulted in the development of a new class of materials viz. polymer–metal

* Corresponding authors.
E-mail addresses: nilanjal17@rediffmail.com (N. Misra), soma_venu@uohyd.ac.in (S. Venugopal Rao).

http://dx.doi.org/10.1016/j.optlastec.2015.11.004
0030-3992/

nanocomposites which combine the properties of both the inorganic and polymer components thereby yielding enhanced or completely new properties [15]. The polymer matrix provides the platform for maintaining the size, shape and dispersion of the metal nanoparticles – parameters which play a vital role in deciding the properties exhibited by the particles. The NLO properties of nanocomposites containing metal nanoparticle fillers arise from the dependence of their refractive index and nonlinear absorption on incident light intensity. Significant enhancement of the NLO response in such nanocomposite materials is often associated with the optical excitation of surface plasmon resonances (SPR) which are collective electromagnetic modes and strongly dependent on the overall morphology of the system [16]. Therefore, such nanoparticles embedded polymer nanocomposites can be effectively applied in novel integrated optoelectronic devices.

Although metal nanoparticle–polymer composites have been conventionally fabricated by mixing preformed nanoparticles with the polymer in solution and casting the composite films (ex-situ), this method puts severe limitations on the homogeneous dispersion of the metal nanoparticles. Therefore, in recent years focus has been shifted to the in situ generation of metal nanoparticles in the polymer matrices [17,18]. One of the methods which has ascended to the fore front in the process is the radiation induced synthesis of polymer nanocomposites. Compared to conventional techniques, the major advantages of using high energy electron beam or gamma irradiation for simultaneous reduction and polymer curing are that they offer a pollution-free work environment, high efficiency and throughput, long service life, uniform cross-linking degree, and excellent heat-resistance and cold-resistance properties. The variation of parameters such as radiation dose, dose rate and metal/polymer ratio facilitates control over the size and dispersion of the metal nanoparticles as well as the overall properties of the nanocomposite material. In this work, we report the fabrication of flexible silver nanoparticles–polyurethane acrylate based polymer nanocomposite films (PNCs) via electron beam irradiation route in an attempt to introduce optical limiting properties in the radiation cured polymer coating films. Aliphatic urethane acrylate was used as the matrix owing to its unique properties, including excellent abrasion resistance, flexibility, hardness, chemical resistance, solvent resistance, and light stability [19]. The PNC samples were tested for their optical limiting properties using an Nd-YAG laser operating at third harmonic wavelength of 355 nm with 25 ns pulse duration and 10 Hz repetition rate. Furthermore, the NLO coefficients of these films were extracted from the standard Z-scan experiments achieved with both picosecond (~2 ps, 1 kHz, 800 nm) and femtosecond (~150 fs, 100 MHz, 800 nm) pulses [20]. Both open aperture and closed aperture data were recorded for retrieving the real and imaginary parts of the third order NLO susceptibility, $\chi^{(3)}$. We have attempted to correlate the obtained NLO results and coefficients in terms of the Ag doping concentration. In both the cases, we observed strong NLO coefficients from the Z-scan data indicating the potential of such nanocomposite system in photonic applications.

2. Experimental

2.1. Materials

Silver nitrate (> 99% purity), Thiophene and Trimethylolpropanetriacrylate (TMPTA) were procured from Sigma Aldrich. Aliphatic urethane acrylate (AUA, Cognis) and Montmorillonite Clay (Cloisite 30B, Southern Clay) were used as received.

2.2. Sample preparation

Different concentrations (w/v) of the precursor ion (Ag^+) solution were added to an optimized mixture of AUA and TMPTA. To achieve uniform dispersion of the filler in the oligomer matrix, each of the samples was subjected to probe ultrasonication (400 W) for 1 h. The formulations obtained were coated onto glass substrates and subjected to electron beam (EB) irradiation technique at ILU6, Vashi, BARC, operated at 2 MeV with power output of 20 kW for a total absorbed dose of 200 kGy to obtain non-tacky, homogeneous thin films. The thickness of the EB cured coatings was found to be ~100 μm as estimated by a thickness gauge 'coat measure M12' (Yuyutsu, Japan).

2.3. UV–visible spectroscopy

The UV–visible absorption spectra were recorded on a UV–visible spectrophotometer (Evolution 300, Thermoelectron, UK) in the wavelength region of 250–800 nm with resolution of 1 nm. The samples were cut into small rectangular sheets, fixed vertically into the sample holder and analyzed in the absorbance mode with a control polymer film of identical dimension as the sample.

2.4. Transmission electron microscopy (TEM)

Transmission Electron Microscopy (TEM) studies were performed on an energy filtering transmission electron microscope (EF-TEM, LIBRA 120, Carl Zeiss) with an accelerating voltage of 120 kV in order to determine the shape and size of the nanofillers. Prior to analysis, the samples were cut into thin sections using an ultramichrotome and placed on the Cu TEM grids.

2.5. Scanning electron microscopy (SEM)

The bulk morphologies of the EB radiation cured polymer coatings were investigated by SEM analysis using field emission scanning electron microscope (JEOL JSM7600) at acceleration voltages of 0.6 kV using a secondary electron detector. The sample cross-sections were pasted onto a conducing surface using silver paste and coated with gold in ion sputter coater, before recording the SEM image.

2.6. NLO Studies

The optical limiting studies were carried out using an Nd-YAG laser operated at third harmonic wavelength of 355 nm (25 ns, 10 Hz) as the excitation source. Samples were mounted on a metal frame and the laser beam focused at the center of the sample for pre-determined time intervals at different incident laser powers till complete burn out of the samples was observed.

The complete experimental details of ps Z-scan were reported elsewhere [21–30]. Briefly, ~2 ps pulses were generated from a regenerative amplifier (Coherent, Legend) seeded by an oscillator (Coherent, Micra). The amplifier was operated at 1 kHz repetition rate and 800 nm and the peak intensities used typically were 16–32 GW/cm^2. The lower peak intensities of the samples were taken into account for the analysis of closed aperture data. A beam diameter of ~3 mm was focused using 20 cm focal length plano-convex lens into the sample. The estimated Rayleigh range calculated was $\sim 3.4 \pm 0.4$ mm. In the fs Z-scan [23,25] ~150 fs pulses with 80 MHz repetition rate were delivered from a tunable oscillator (Chameleon, Coherent), operated at central wavelength 800 nm. An input beam diameter of ~3 mm and plano convex lens (focal length 10 cm) were used to focus on to the sample. The coresponding Rayleigh range was calculated to be 1.4 ± 0.2 mm. A set of neutral density filters were used to attenuate the input

energy of laser pulses and to ensure that there was negligible contribution from higher order nonlinear effects. The peak intensities used were typically 0.1–0.3 GW/cm^2 and all the scans were recorded at lower peak intensities. A 10 μm resolution translation stage was used to mechanically scan the sample with a step size of 1 mm. The corresponding output transmittance was recorded using a power meter and a 5 cm plano convex lens combination. An aperture was placed in front of the lens for closed aperture Z-scan. The experiments were repeated for three times and the best data was taken from different sets for all the samples and was fitted for two-photon absorption.

3. Results and discussion

3.1. Fabrication of nanocomposite films

The precursor ion stock solution of silver nitrate was prepared in methanol as the solvent owing to its ready miscibility with the oligomer-diluent reaction mixture. AUA was chosen as the oligomer due to the high flexibility and superior mechanical properties offered by polyurethane acrylate. TMPTA serves as the reactive diluent as well as a crosslinking agent by virtue of its three functional acrylate groups, which form connecting bridges between the PUA polymeric chains through a free radical based polymeric chain reaction initiated by EB irradiation. The AUA–TMPTA ratio was maintained at 4:1 to achieve optimum viscosity and to ensure maximum crosslinking between the polymeric chains. Three different volumes of Ag^+ ion solution were added to 5 g AUA–TMPTA mixtures to arrive at final Ag^+ ion concentrations of 8, 15 and 25 mM. Radiation doses were optimized at 200 kGy to achieve non tacky homogeneous polymeric films in which Ag nanoparticles were generated in situ via radiolytic reduction of the precursor Ag^+ ions.

3.2. Characterization of Ag PNC films

The formation of Ag nanoparticles in the polymer matrix was confirmed by the bright yellow color generated in the film as compared to the colorless control polymer film. Fig. 1 illustrates the UV–visible absorption data of the films depicting characteristic narrow Surface Plasmon Resonance (SPR) band of Ag nanoparticles at ~420 nm, thereby confirming the formation of more or less uniform sized, spherical silver nanoparticles within the polymer matrix. It is known that the nature of external environment significantly influences the spectral behavior of the LSPR band of metal nanoparticles [31]. The spectral behavior in this case can, therefore, be attributed to the effect of the solid polymer matrix surrounding the in situ generated Ag NPs, which can significantly alter the dielectrics of the system. The collective dipolar interactions between nanoparticles can cause a broadening and red-shift of the absorption band under high filler concentrations. The TEM image of the Ag NPs clearly indicated formation of uniformly dispersed spherical nanoparticles with average particle size of 8–10 nm, which was further substantiated by the FE-SEM image. Therefore, the probability of spectral broadening arising due to large size variation can be ruled out. The possibility of ageing or agglomeration of the Ag NPs is also minimal since the polyurethane acrylate matrix acts as a highly efficient stabilizing agent which can prevent the Ag NPs formed from undergoing rapid agglomeration. A previous work, carried out by Ganeev et al. [31], involved dispersion of the Ag NPs in a liquid phase, which provided an entirely different medium compared to a solid matrix. Also, the low stability of their system resulted in a gradual aggregation of Ag NPs, which manifested as a red shift in the LSPR band. Such a process of gradual aggregation of Ag NPs is not evident in our system. The intensity of the LSPR band increased proportionately with increase in the Ag concentration of the PNC film. Fig. 2(a) presents the TEM image of the in situ generated Ag nanoparticles. TEM analysis clearly indicated formation of

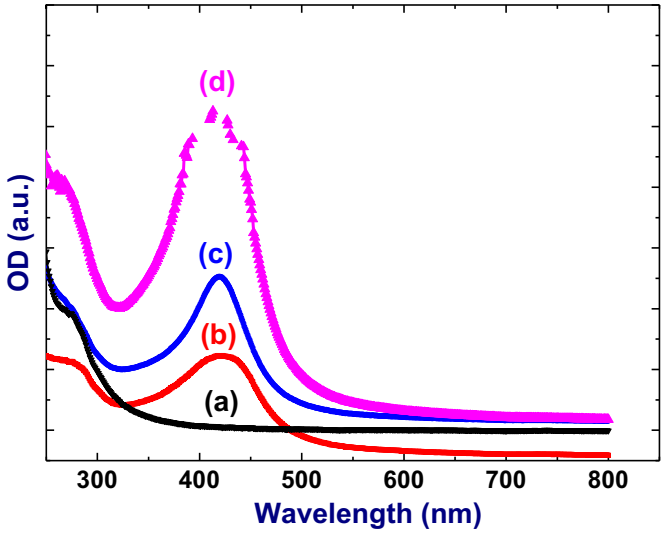

Fig. 1. UV–visible spectra of (a) control PNC film and PNC films containing (b) 8 mM (c) 15 mM and (d) 25 mM Ag NPs as fillers.

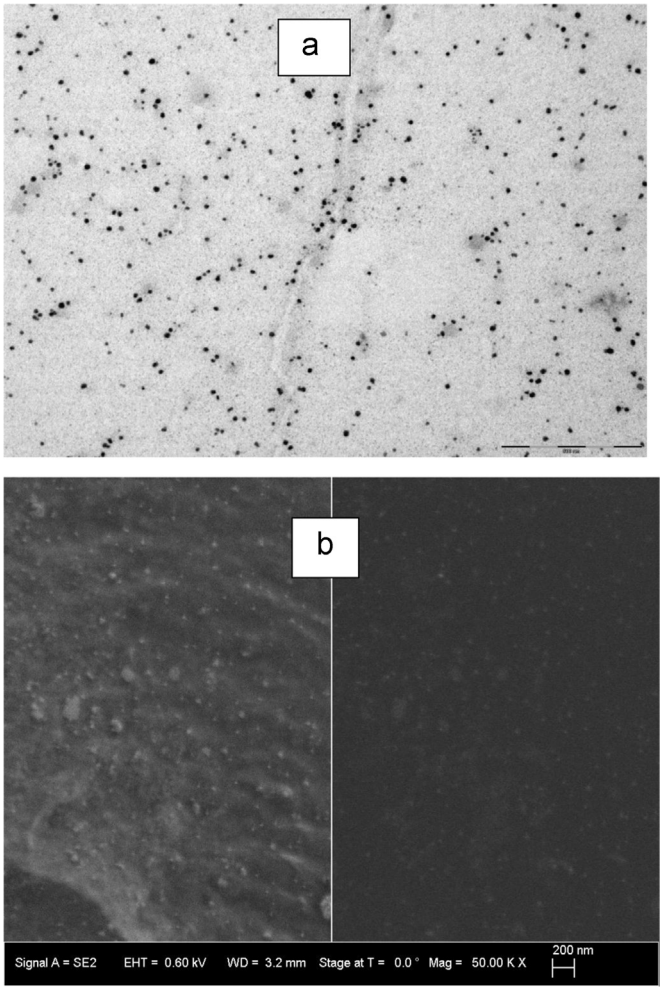

Fig. 2. (a) TEM image of PNC film containing 25 mM Ag NPs as filler (b) FE-SEM image of PNC film containing 25 mM Ag NPs as filler.

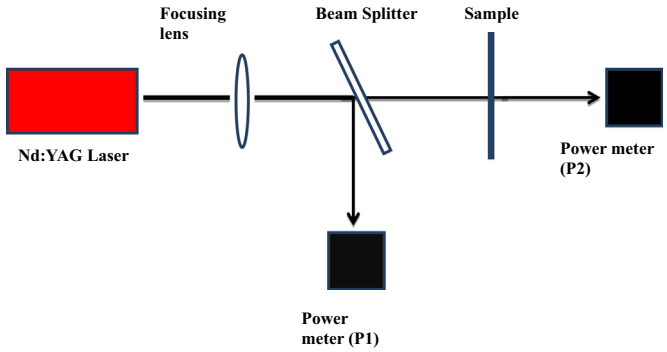

Fig. 3. Schematic of set up for optical limiting study of PNC films.

uniformly dispersed spherical nanoparticles with an average particle size of 8–10 nm. FE-SEM image shown in Fig. 2(b) also confirms the formation of uniform sized spherical Ag nanoparticles embedded in the polymer matrix.

3.3. Nanosecond optical limiting properties of Ag PNC films

The optical-limiting behavior of the composites with different Ag NPs concentrations were measured using Nd:YAG laser with 25 ns pulse duration and 355 nm wavelength. The experiment set up is shown in Fig. 3. The sample was mounted on a metal frame and the laser beam focused on the sample surface with a spot size of 1.0 mm diameter. The incident and transmitted energy were detected simultaneously by two power meters (P1, P2). The film was exposed to the laser beam for duration of 10 s. The incident laser power was increased after every 10 s exposure till complete burnout of the samples was observed. The result is shown in Fig. 4, which distinctly highlights the optical-limiting effect of PNC containing 25 mM Ag NPs as the nanofiller (Ag25). At very low output energy, the response of the composite was linear to the input energy. The linear transmittance was found to be approximately 82% while the limiting or threshold input fluence beyond which the sample stopped transmitting the laser beam was calculated to be 3.8×10^{-2} J/cm^2. Similar trends were observed for composites containing 8 mM and 15 mM Ag NPs as filler. This clearly indicates that the transmittance and threshold fluence of the films was independent of the concentration of the nanofillers in the range under study; with the common base polymer matrix acting as the deciding factor in determining the extent of transmittance. In order to study the effect of the exposure duration on the optical limiting effect of the PNC film, similar experiments were carried out by limiting the time of exposure to 1 s. Fig. 4 shows the variation in optical limiting characteristics for PNC containing 25 mM Ag NPs with change in the time of exposure. Exposure for 1 s led to significant improvement in the optical limiting property of the material, which was manifested in the decrease in threshold fluence from 3.8×10^{-2} J/cm^2 to 1.2×10^{-2} J/cm^2. The dynamic range, which is defined as the ratio of the maximum input fluence till which material displays optical limiting behavior to the threshold fluence, was also found to increase from ~22 to ~80. In other words, exposure for lesser durations not only led to an early cut off for the laser transmission but also increased the overall lifetime of the material. This can be explained on the basis of the fact that continuous exposure for long durations led to accumulation of laser power within a small area (determined by the beam diameter) thereby culminating in rapid degradation of the product. In addition to Ag NPs as fillers, the effect of addition of fillers such as Thiophene (Ag25T) and modified montmorilonite clay (Cloisite 30B) (Ag25C) in conjunction with Ag NPs, on the optical limiting behavior, was also studied. The results are highlighted in Fig. 5. It was observed that for exposure of 1 s, change in the filler concentration did not lead to any change in the threshold fluence of the materials. However, the presence of Cloisite 30B as additional filler led to an early damage of the films, resulting in a narrower dynamic range compared to the other two composite films. On the other hand Thiophene/Ag based films (Ag25T) exhibited increased output fluence at higher input fluences.

3.4. NLO studies using fs aND PS pulses

We have also investigated third order optical nonlinearities using fs (~150 fs, 800 nm) and ps (~2 ps, 800 nm) excitations at 800 nm using the standard Z-scan technique. The potential of samples for optical limiting applications in ps/fs time domains could be estimated from the open aperture results of ps/fs Z-scan, whereas ps/fs closed aperture Z-scan results can appraise its potential in optical switching kind of applications. From the ps and fs open aperture data we obtained TPA coefficients by fitting the experimental data. Closed aperture Z-scan data was fitted and n_2 values were retrieved. The sign and magnitude of nonlinear

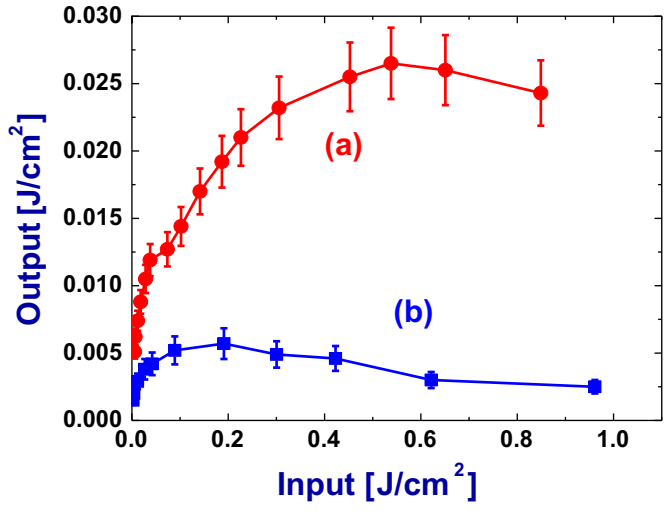

Fig. 4. Plot of output fluence (in J/cm^2) versus input fluence (in J/cm^2) for PNC film containing 25 mM Ag NPs (Ag25) as filler for exposure durations of (a) 10 s and (b) 1 s. Solid lines are a guide to the eye.

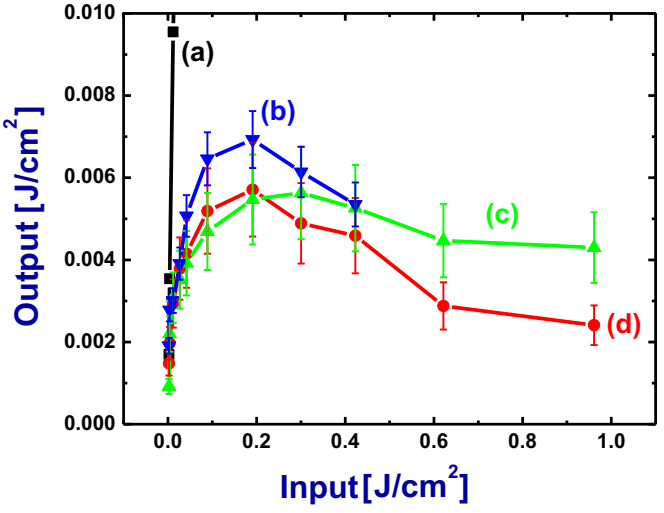

Fig. 5. Plot of output fluence (in J/cm^2) versus input fluence (in J/cm^2) for (a) control PNC film and PNC films containing (b) Thiophene/Ag NPs (Ag25T), (c) Cloisite 30B/Ag NPs (Ag25C) and (d) 25 mM Ag NPs (Ag25) as filler (exposure durations=1 s). Solid lines are a guide to the eye.

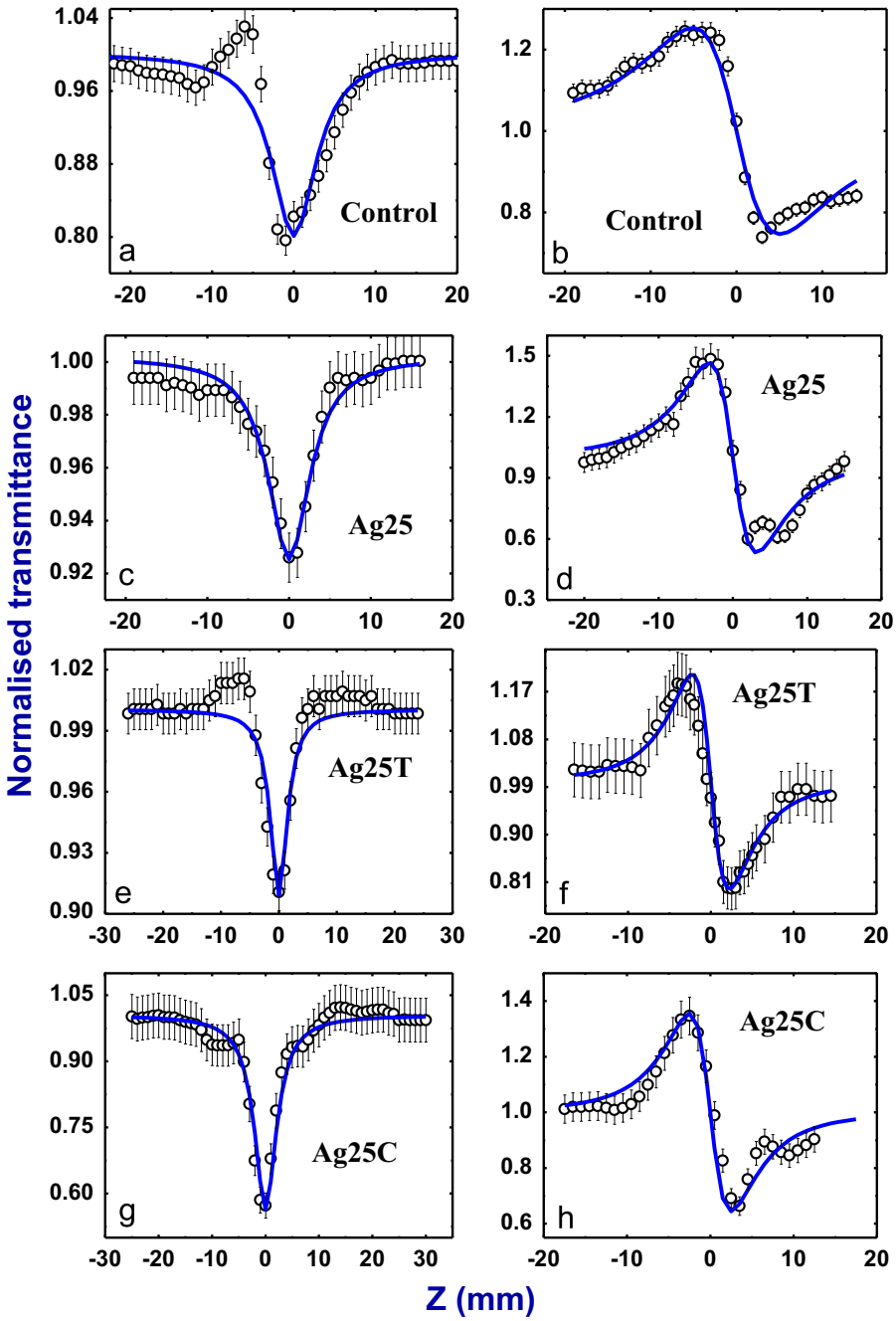

Fig. 6. (a), (c), (e), and (g) depicts fs open aperture (open circles) data and their two-photon absorption fits (solid, blue lines) for control, Ag25, Ag25T, and Ag25C films, respectively. (b), (d), (f), and (h) presents fs closed aperture Z-scan data (open circles) and their theoretical fits (solid, blue lines) for control, Ag25, Ag25T, and Ag25C films, respectively. (For interpretation of the references to color in this figure legend, the reader is referred to the web version of this article.)

refractive index (n_2), two-photon absorption (TPA) coefficients (β) and third-order NLO susceptibility [$\chi^{(3)}$] were extracted from the Z-scan data.

Fig. 6(a), (c), (e), and (g) depict the fs open aperture (open circles) data and their two-photon absorption fits (solid, blue lines) for control, Ag25, Ag25T, and Ag25C films, respectively, while Fig. 6(b), (d), (f), and (h) present fs closed aperture Z-scan data (open circles) and their theoretical fits (solid, blue lines) for control, Ag25, Ag25T, and Ag25C films, respectively. We obtained two sets of data for each film and the best data was chosen for the fitting of open and closed aperture Z-scan. In this case Ag25C and control films had demonstrated highest TPA coefficients of 140×10^{-10} and 25×10^{-10} cm/W, respectively, whereas control and Ag25 films demonstrated highest nonlinear refractive index values with magnitudes of 2.8×10^{-11} cm^2/W and 2.1×10^{-11} cm^2/W, respectively. All the samples showed a self-defocusing effect (negative nonlinearity) which is evident from the signatures in closed aperture Z-scan. Surprisingly the control film depicted strong nonlinearities in both open and closed aperture cases. This could be understood and explained as follows. If the control film has strong negative nonlinearity while the other films (with NPs) possess positive nonlinearity then the overall n_2 values will be lower than that of the control film. Similarly, if the control film has strong TPA whereas the other films have saturable absorption then the overall TPA coefficients of other films will be lower than that of the control film. Since the pulses are of 100 MHz repetition rate, thermal effects are expected to dominate in the overall nonlinearities. The difference in the thermal coefficients of

Table 1
Summary of fs NLO coefficients obtained using open and closed aperture Z-scan at 800 nm.

Femtosecond NLO coefficients (800 nm, 80 MHz, ~150 fs)								
Sample	**Input power (mW)**	L_{eff2} ($\times 10^{-4}$)	β ($\times 10^{-10}$ cm/W)	n_2 ($\times 10^{-11}$ cm^2/W)	Re $\lvert\chi^{(3)}\rvert$ (esu)	Im $\lvert\chi^{(3)}\rvert$ (esu)	$\lvert\chi^{(3)}\rvert$ (esu)	$\lvert\chi^{(3)}\rvert$ (S.I.)
Control [n_o=1.48]	10	1.4	25	−2.8	-1.5×10^{-09}	3.5×10^{-11}	1.5×10^{-09}	2.2×10^{-17}
Ag25 [n_o=1.5]	15	1.4	7.2	−2.1	-1.2×10^{-09}	1.0×10^{-12}	1.2×10^{-09}	1.7×10^{-17}
Ag25T [n_o=1.48]	8	1.2	18	−1.5	-8.3×10^{-10}	2.6×10^{-12}	8.3×10^{-10}	1.2×10^{-17}
Ag25C [n_o=1.48]	13	1.1	140	−1.8	-9.9×10^{-10}	1.9×10^{-11}	9.9×10^{-10}	1.4×10^{-17}

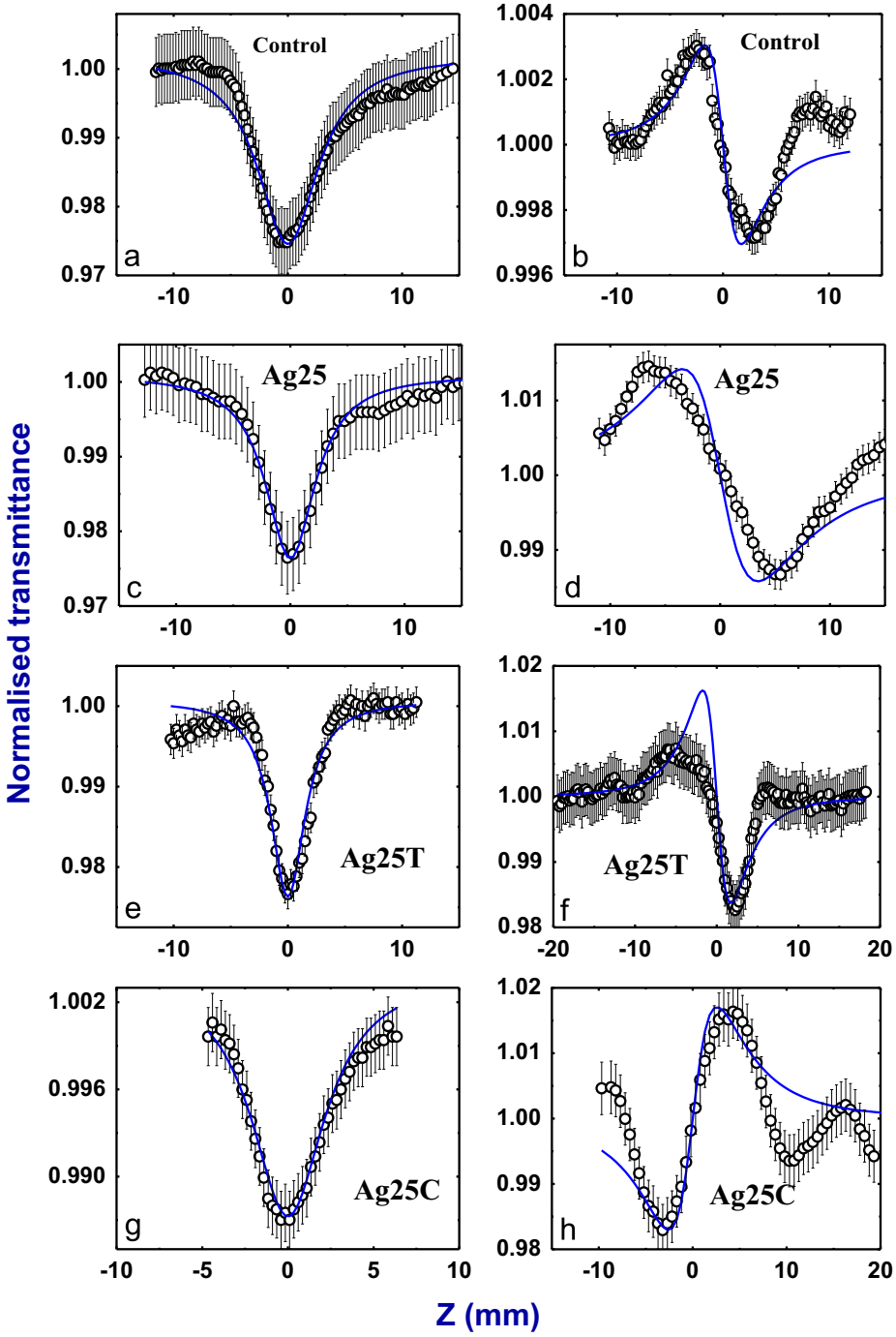

Fig. 7. (a), (c), (e), and (g) depicts ps open aperture (open circles) data and their two-photon absorption fits (solid, blue lines) for control, Ag25, Ag25T, and Ag25C films, respectively. (b), (d), (f), and (h) presents ps closed aperture Z-scan data (open circles) and their theoretical fits (solid, blue lines) for control, Ag25, Ag25T, and Ag25C films, respectively.

Table 2
Summary of ps NLO coefficients obtained using open and closed aperture Z-scan at 800 nm.

Picosecond NLO coefficients (800 nm, 1 kHz, ~2 ps)							
Sample	**Power (mW)**	**β ($\times 10^{-10}$ cm/W)**	**n_2 ($\times 10^{-15}$ cm^2/W)**	**Re $\lvert\chi^{(3)}\rvert$ (esu)**	**Im $\lvert\chi^{(3)}\rvert$ (esu)**	**$\lvert\chi^{(3)}\rvert$ (esu)**	**$\lvert\chi^{(3)}\rvert$ (S.I)**
Control [n_o=1.48]	1.5	0.015	−0.90	-5.0×10^{-14}	2.1×10^{-15}	5.0×10^{-14}	7.0×10^{-22}
Ag25 [n_o=1.5]	1.2	0.016	−2.20	-1.2×10^{-13}	5.8×10^{-15}	1.2×10^{-13}	1.8×10^{-21}
Ag25T [n_o=1.48]	1.2	0.016	−2.75	-1.5×10^{-13}	5.8×10^{-15}	1.5×10^{-13}	2.1×10^{-21}
Ag25C [n_o=1.48]	1.2	0.013	3.16	1.7×10^{-13}	1.8×10^{-15}	1.7×10^{-13}	2.4×10^{-21}

the control film and that of films with Ag NPs can also influence the values of the observed NLO coefficients. This is evident from the magnitudes of n_2, β, and $\chi^{(3)}$, which were in the range of $\sim10^{-11}$ cm^2/W, $\sim10^{-9}$ cm/W, $\sim10^{-9}$ e.s.u., respectively. The real and imaginary parts of nonlinear susceptibility along with their signs and magnitude are summarized in Table 1.

Fig. 7(a), (c), (e), and (g) depict the ps (1 kHz repetition rate) open aperture (open circles) data and their two-photon absorption fits (solid, blue lines) for control, Ag25, Ag25T, and Ag25C films, respectively while Fig. 7(b), (d), (f), and (h) present ps closed aperture Z-scan data (open circles) and their theoretical fits (solid, blue lines) for control, Ag25, Ag25T, and Ag25C films, respectively. All the samples exhibited TPA coupled with a self-defocusing effect in the ps regime. Ag25C, however, depicted self-focusing effect. Control film, Ag25, Ag25T films depicted a negative nonlinearity with peak-valley signature whereas, Ag25C depicted a positive nonlinearity signature. Ag25 showed a strong TPA coefficient of 0.016×10^{-10} cm/W, while n_2 was the highest in case of Ag25C, possessing a value 3.16×10^{-15} cm^2/W with a positive lensing effect. Although the magnitude of β was similar for all the samples, the values of n_2 increased sequentially from control film to Ag25, Ag25C and Ag25T. Since the pulses used were of ~2 ps duration, the observed n_2 values could have major contribution from electronic nonlinearities. We had ensured that the closed aperture data was recorded with very low peak intensities to avoid any nonlinear absorption contributions. The fittings to the experimental data clearly suggested the presence of TPA. A strong absorption peak in the region at 400 nm could possibly have resulted in TPA excitation. Since the pulses used were ~2 ps we have ignored the contribution of excited state absorption (ESA), though one cannot completely rule out the possibility [29]. The TPA coefficient presented in the ps case is an effective TPA including the ESA contributions. The values of n_2, β, and $\chi^{(3)}$ values for all the samples using 2 ps, 1 kHz and 800 nm are calculated and summarized in Table 2. The NLO coefficient values presented here for our films are on par with some of the recently reported molecules. For example, Sathyavathi et al. [32] studied NLO properties of biosynthesized silver nanoparticles and obtained n_2 and $\chi^{(3)}$ values of 10^{-13} cm^2/W and 10^{-9} e.s.u., respectively. Ganeev et al. [31] studied NLO properties of silver nanoparticles prepared by laser ablation and obtained values of 10^{-13} cm^2/W and 10^{-8} e.s.u. for n_2 and $\chi^{(3)}$, respectively. Tripathi et al. [33] studied continuous wave (cw) NLO properties of Ag–CdSe/PVA hybrid nanocomposite and obtained large values of n_2 and $\chi^{(3)}$ (10^{-5} cm^2/W and 10^{-9} m^2/V^2) which are expected for cw excitation. Lee et al. [34] investigated the NLO properties of Ag nanoparticles in polymer matrix and obtained two-photon absorption coefficient of 10^{-7} cm/W for fs excitation. Liu et al. [35] obtained $\chi^{(3)}$ value of 10^{-8} e.s.u. for nanoparticle–polymer composites incorporating organic (hyperbranched polymer)–metallic (silver) nanoparticle complex. Deng et al. [36] reported n_2 and β values of 10^{-15} m^2/W and 10^{-8} m/W, respectively, for Ag nanocomposite polymer films prepare in situ with ns excitation at 532 nm.

4. Conclusions

We have successfully fabricated Ag nanoparticles dispersed in aliphatic urethane acrylate polymer matrix (nanocomposites) using electron beam curing technique. The morphologies of these films were studied using the TEM and FESEM imaging techniques. The films were also characterized using UV–visible absorption spectroscopic techniques. The NLO properties of these films were investigated using ns, ps, and fs pulses. Ns optical limiting studies suggest these polymers are good optical limiters. Ps (1 kHz pulses) NLO coefficients were evaluated from Z-scan measurements. The magnitudes of n_2, β, and $\chi^{(3)}$ were in the range of $\sim10^{-15}$ cm^2/W, $\sim10^{-12}$ cm/W, $\sim10^{-15}$ e.s.u., respectively. Large NLO coefficients were obtained with fs pulse excitation (100 MHz repetition rate). The magnitudes of n_2, β, and $\chi^{(3)}$ in the fs case were in the range of $\sim10^{-11}$ cm^2/W, $\sim10^{-9}$ cm/W, $\sim10^{-9}$ e.s.u., respectively. Our detailed studies propose that these films are potential candidates for various NLO and photonic applications.

Acknowledgments

We acknowledge the continuous financial support from Defense Research Development Organization, India through the grant ERIP/ER/1109003/M/01/1338/1302/D(R&D).

References

[1] Y.P. Sun, J.E. Riggs, Organic and inorganic optical limiting materials. From fullerenes to nanoparticles, Int. Rev. Phys. Chem. 18 (1999) 43–90.
[2] S. Porel, N. Venkatram, D. Narayana Rao, T.P. Radhakrishnan, In situ synthesis of metal nanoparticles in polymer matrix and optical limiting application, J. Nanosci. Nanotechnol. 7 (2007) 1–6.
[3] J. Wang, K.-S. Liao, D. Früchtl, Y. Tian, A. Gilchrist, N.J. Alley, E. Andreoli, B. Aitchison, A.G. Nasibulin, H.J. Byrne, E.I. Kauppinen, L. Zhang, W.J. Blau, S. A. Curran, Nonlinear optical properties of carbon nanotube hybrids in polymer dispersions, Mater. Chem. Phys. 133 (2012) 992–997.
[4] Y. Chen, Y. Lin, Y. Liu, J. Doyle, N. He, X.D. Zhuang, J.R. Bai, W.J. Blau, Carbon nanotube-based functional materials for optical limiting, J. Nanosci. Nanotechnol. 7 (2007) 1268–1283.
[5] J. Wang, W.J. Blau, Inorganic and hybrid nanostructures for optical limiting, J. Opt. A: Pure Appl. Opt. 11 (2009) 024001.
[6] J. Wang, Y. Chen, W.J. Blau, Carbon nanotubes and nanotube composites for nonlinear optical devices, J. Mater. Chem. 19 (2009) 7425–7443.
[7] W. Blau, H. Byrne, W.M. Dennis, J.M. Kelly, Reverse saturable absorption in tetraphenylporphyrins, Opt. Commun. 56 (1985) 25–29.
[8] L. Yang, D.H. Osborne, R.F. Haglund, R.H. Magruder, C.W. White, R.A. Zuhr, H. Hosono, Probing interface properties of nanocomposites by third-order nonlinear optics, Appl. Phys. A: Mater. Sci. Process 62 (1996) 403–415.
[9] S.C. Mehendale, S.R. Mishra, K.S. Bindra, M. Laghate, T.S. Dhami, K.C. Rustagi, Nonlinear refraction in aqueous colloidal gold, Opt. Commun. 133 (1997) 273–276.
[10] Y. Hamanaka, K. Fukuta, A. Nakamura, Enhancement of third-order nonlinear optical susceptibilities in silica-capped Au nanoparticle films with very high concentrations, Appl. Phys. Lett. 84 (2004) 4938.
[11] R.A. Ganeev, A.I. Ryasnyansky, Nonlinear optical characteristics of nanoparticles in suspensions and solid matrices, Appl. Phys. B: Lasers Opt. 84 (2006) 295–302.
[12] R.A. Ganeev, M. Suzuki, M. Baba, M. Ichihara, H. Kuroda, Low- and high-order nonlinear optical properties of Au, Pt, Pd, and Ru nanoparticles, J. Appl. Phys.

103 (2008) 063102.
[13] H.I. Elim, J. Yang, J. Lee, Observation of saturable and reverse-saturable absorption at longitudinal surface plasmon resonance in gold nanorods, Appl. Phys. Lett. 88 (2006) 083107.
[14] O.M. Folarin, E.R. Sadiku, A. Maity, Polymer-noble metal nanocomposites: review, Int. J. Phys. Sci. 6 (21) (2011) 4869–4882.
[15] Z. Zhang, M. Han, One-step preparation of size-selected and well dispersed silver nanocrystals in polyacrylonitrile by simultaneous reduction and polymerization, J. Mater. Chem. 13 (2003) 641–643.
[16] U. Kreibig, M. Vollmer, Optical Properties of Metal Clusters, Springer, Berlin, 1995.
[17] S. Porel, S. Singh, S.S. Harsha, D.N. Rao, T.P. Radhakrishnan, Nanoparticle-embedded polymer: in situ synthesis, free-standing films with highly monodisperse silver nanoparticles and optical limiting, Chem. Mater. 17 (2005) 9–12.
[18] M.G. Murali, U. Dalimba, K. Sridharan, Synthesis, characterization, and nonlinear optical properties of donor–acceptor conjugated polymers and polymer/Ag nanocomposites, J. Mater. Sci. 47 (2012) 8022–8034.
[19] X. Wang, W. Xing, L. Song, B. Yu, Y. Hu, G.H. Yeoh, Preparation of UV-curable functionalized graphene/polyurethane acrylate nanocomposite with enhanced thermal and mechanical behaviors, React. Funct. Polym. 73 (2013) 854–858.
[20] M. Sheik-Bahae, A.A. Said, T.H. Wei, D.J. Hagan, E.W. Van Stryland, IEEE J. Quantum Electron. 26 (1990) 760–769.
[21] S. Hamad, Surya P. Tewari, L. Giribabu, S. Venugopal Rao, Picosecond and femtosecond optical nonlinearities of novel corroles, J. Porphyr. Phthalocyanines 16 (2012) 140–148.
[22] S.J. Mathews, S. Chaitanya Kumar, L. Giribabu, S. Venugopal Rao, Nonlinear optical and optical limiting properties of phthalocyanines in solution and thin films of PMMA studied using a low power He–Ne laser, Mater. Lett. 61 (2007) 4426–4431.
[23] N. Venkatram, D. Narayana Rao, L. Giribabu, S. Venugopal Rao, Femtosecond nonlinear optical properties of alkoxy phthalocyanines at 800 nm studied using Z-Scan technique, Chem. Phys. Lett. 464 (2008) 211–215.
[24] N.V. Krishna, V.K. Singh, D. Swain, S. Venugopal Rao, L. Giribabu, Optical, electrochemical, third order nonlinear optical, and excited state dynamics studies of *bis*(3,5-trifluoromethyl)phenyl-zinc phthalocyanine, R. Soc. Chem. Adv. 5 (2015) 20810–20817.
[25] S. Umar Pasha, P. Ajay Kumar, M. Ghanashyam Krishna, S. Venugopal Rao, Microstructural manipulation of nonlinear optical response of ZnO films grown by thermal evaporation technique, Mater. Res. Express 1 (2014) 046201.
[26] B. Anand, A. Kaniyoor, D. Swain, T.T. Baby, S. Venugopal Rao, S.S. Sankara Sai, S. Ramaprabhu, R. Philip, Enhanced optical limiting and carrier dynamics in metal oxide-hydrogen exfoliated graphene hybrids, J. Mater. Chem. C 2 (2014) 10116–10123.
[27] D. Swain, R. Singh, V.K. Singh, N.V. Krishna, L. Giribabu, S. Venugopal Rao, Sterically demanded zinc(II)phthalocyanines: synthesis, optical, electrochemical, nonlinear optical, excite state dynamics studies, J. Mater. Chem. C 2 (2014) 1711–1722.
[28] P.T. Anusha, D. Swain, S. Hamad, T. Shuvan Prashant, L. Giribabu, Surya P. Tewari, S. Venugopal Rao, Ultrafast excited state dynamics and third order optical nonlinearities of novel Corroles, J. Phys. Chem. C 116 (2012) 17828–17837.
[29] S. Venugopal Rao, Picosecond nonlinear optical studies of gold nanoparticles synthesized using coriander leaves (*Coriandrum sativum*), J. Mod. Opt. 58 (12) (2011) 1024–1049.
[30] S. Venugopal Rao, T. Shuvan Prashant, T. Sarma, Pradeepta K. Panda, D. Swain, Surya P. Tewari, Two-photon and three-photon absorption in dinaphthoporphycenes, Chem. Phys. Lett. 514 (2011) 98–103.
[31] R.A. Ganeev, M. Baba, A.I. Ryasnyansky, M. Suzuki, H. Kuroda, Characterization of optical and nonlinear optical properties of silver nanoparticles prepared by laser ablation in various liquids, Opt. Commun. 240 (2004) 437–448.
[32] R. Sathyavathi, M. Balamurali Krishna, S. Venugopal Rao, R. Saritha, D. Narayana Rao, Biosynthesis of silver nanoparticles using *Coriandrum Sativum* leaf extract and their application in nonlinear optics, Adv. Sci. Lett. 3 (2) (2010) 138–143.
[33] S.K. Tripathi, R. Kaur, J. Kaur, M. Sharma, Third-order nonlinear optical response of Ag–CdSe/PVA hybrid nanocomposite, Appl. Phys. A 120 (2015) 1047–1057.
[34] G.J. Lee, Y.-P. Lee, C.S. Yoon, Microstructures and linear/nonlinear optical properties of monolayered silver nanoparticles, J. Korean Phys. Soc. 53 (6) (2008) 3818–3822.
[35] X. Liu, K. Matsumura, Y. Tomita, K. Yasui, K. Kojima, K. Chikama, Nonlinear optical responses of nanoparticle–polymer composites incorporating organic (hyperbranched polymer)–metallic nanoparticle complex, J. Appl. Phys. 108 (2010) 07312.
[36] Y. Deng, Y. Sun, P. Wang, D. Zhang, H. Ming, Q. Zhang, In situ synthesis and nonlinear optical properties of Ag nanocomposite polymer films, Thin Solid Films 40 (2008) 911–914.